PHYSICAL REVIEW B **79**, 224117 (2009)

Influence of anisotropic strain on the dielectric and ferroelectric properties of $SrTiO_3$ thin films on $DyScO_3$ substrates

M. D. Biegalski,[1,2] E. Vlahos,[2] G. Sheng,[2] Y. L. Li,[2] M. Bernhagen,[3] P. Reiche,[3] R. Uecker,[3] S. K. Streiffer,[4] L. Q. Chen,[2] V. Gopalan,[2] D. G. Schlom,[5] and S. Trolier-McKinstry[2]

[1]*Center for Nanophase Materials Sciences, Oak Ridge National Laboratory, Oak Ridge, Tennessee 37830, USA*

[2]*Materials Research Institute, Pennsylvania State University, University Park, Pennsylvania 16802, USA*

[3]*Institute for Crystal Growth, D-12489 Berlin, Germany*

[4]*Center for Nanoscale Materials, Argonne National Laboratory, Argonne, Illinois 60439, USA*

[5]*Department of Materials Science and Engineering, Cornell University, Ithaca, New York 14853, USA*

(Received 18 March 2009; revised manuscript received 18 May 2009; published 26 June 2009)

The in-plane dielectric and ferroelectric properties of coherent anisotropically strained $SrTiO_3$ thin films grown on orthorhombic (101) $DyScO_3$ substrates were examined as a function of the angle between the applied electric field and the principal directions of the substrate. The dielectric permittivity revealed two distinct maxima as a function of temperature along the $[100]_p$ and $[010]_p$ $SrTiO_3$ pseudocubic directions. These data, in conjunction with optical second-harmonic generation, show that the switchable ferroelectric polarization develops first predominantly along the in-plane axis with the larger tensile strain before developing a polarization component along the perpendicular direction with smaller strain as well, leading to domain twinning at the lower temperature. Finally, weak signatures in the dielectric and second-harmonic generation response were detected at the $SrTiO_3$ tilt transition close to 165 K. These studies indicate that anisotropic biaxial strain can lead to new ferroelectric domain reorientation transitions that are not observed in isotropically strained films.

DOI: 10.1103/PhysRevB.79.224117 PACS number(s): 77.80.−e, 77.84.−s, 68.55.−a

I. INTRODUCTION

The onset of polarization in ferroelectric materials is accompanied by a spontaneous strain. As a result, applied strains influence the stability of the ferroelectric phases, the transition temperature, and the observed domain state, as well as the dielectric and electromechanical properties.[1–13] In thin films, in-plane strain can shift the ferroelectric transition temperature by up to hundreds of degrees, in accordance with thermodynamic theory.[7–13] The existing thermodynamic predictions assume a uniform in-plane biaxial strain state, which is reasonable for films on cubic substrates or films with a significant level of relaxation. When grown on nonsquare surface nets, however [e.g., (101) $NdGaO_3$, (101) $DyScO_3$ or any other non cubic substrate], the ferroelectric films are subjected to nonuniform in-plane biaxial strain.[14] For (101) $DyScO_3$ this anisotropy was expected to be very small; however, the (101) $DyScO_3$ single crystals used in our studies show much larger differences between the two in-plane lattice constants[15–17] than those previously reported in the literature,[18] increasing the anisotropy in the system. In this work, the effects of the asymmetric biaxial tensile strain state on the dielectric and ferroelectric properties of $SrTiO_3$ thin films on (101) $DyScO_3$ are determined.

II. EXPERIMENTAL PROCEDURE

$SrTiO_3$ films were grown on (101) $DyScO_3$ substrates by reactive molecular-beam epitaxy[19] to thicknesses of 250 and 500 Å. The films were deposited using a shuttered growth technique described elsewhere.[20] The stoichiometry was optimized *in situ* using reflection high-energy electron diffraction.[14] The structure, including the lattice parameters of the $SrTiO_3$ thin films, was characterized using a Philips X'pert MRD four-circle diffractometer using Cu $K\alpha_1$ radiation with a four-bounce germanium monochromator and a two bounce germanium analyzer crystal. The strain states of these films were calculated from their lattice constants using 3.905 Å as the fully relaxed lattice constant of $SrTiO_3$.[21]

In order to investigate the asymmetry of the in-plane dielectric properties, interdigitated electrodes (IDT) were employed with angles of 0°, 15°, 30°, 45°, 60°, and 90° with respect to the *b* axis (the long axis) of the $DyScO_3$ substrate. The orientation of the electric field for these electrodes is largely perpendicular to the finger length. By varying the orientation of the interdigitated electrodes, properties can be probed at various angles in the plane of the film. These IDT electrode structures were patterned photolithographically with Cr/Au using a lift-off process. The dielectric measurements were made using an HP4284A LCR meter with a Desert Cryogenics probe station and the dielectric constants were extracted using a conformal mapping technique.[22] The polarization switching was also measured using a positive-up negative-down (PUND) measurement on the same probe station with an Aixacct TF2000 ferroelectric analyzer.[23]

To complement the electrical measurements, optical second-harmonic generation (SHG) measurements were used to determine the point-group symmetry and the direction of ferroelectric polarization. The SHG experiment was carried out using a fundamental beam of 800 nm that was focused on the thin film and the input polarization was rotated in the plane of the film. The intensity of the second harmonic at 400 nm was recorded along the $x[100]_p$, $y[010]_p$, $x'[110]_p$, and $y'[\bar{1}10]_p$ directions, where *p* denotes the pseudocubic indices of the perovskite unit cell. A bare substrate was used as a reference to verify that the observed SHG signal was generated only from the thin film.

III. RESULTS AND DISCUSSION

A. Structure and epitaxy

The rocking curve widths of the 002 $SrTiO_3$ film peaks are extremely sharp with full width half maxima of less than 7 arc sec (0.0019°).[14,26] Due to slight variability in the $DyScO_3$ substrate lattice parameters, this work will focus on two films (a 250 Å and a 500 Å thick film) though the data presented here are consistent with all samples measured. The 250 Å thick film was fully coherent with the substrate, with a strain of $1.06 \pm 0.03\%$ along the longer $DyScO_3$ in-plane direction [010] and $1.03 \pm 0.03\%$ along the shorter in-plane direction $[10\bar{1}]$. The 500 Å thick films show slight structural relaxation with a strain state of $1.01 \pm 0.03\%$ and $0.99 \pm 0.03\%$ for the longer and shorter axes, respectively. (It is important to note that while our absolute error on the strain state is 0.03% the relative difference in strain is much smaller.) Both films exhibit $(001)_p$ out-of-plane oriented $SrTiO_3$. The epitaxial relationship is $(001)_p$ $SrTiO_3 \| (101)DyScO_3$ and $[010]_p$ $SrTiO_3 \| [010]DyScO_3$.[24–26]

B. Dielectric properties

1. Orientation dependence of dielectric properties

Using IDT electrodes with various orientations, the dielectric properties were probed along different in-plane directions. Figure 1 shows the in-plane dielectric constant at 5 kHz as a function of temperature for several angles. Intriguingly, two distinct dielectric maxima along the two principal $[100]_p$ in-plane directions are observed. These two peaks appear near 260 K (labeled T_1) along the longer in-plane direction (0°) and 210 K (labeled T_2) for the shorter in-plane direction (90°). Data at intermediate angles sample both peaks. Comparable behavior is observed for the dielectric loss [Fig. 1(b)], though the T_{max} (tan δ) occur at somewhat lower temperatures. Both peaks show the frequency dispersion characteristic of relaxor ferroelectrics.

The magnitudes of the permittivity, the frequency dispersion in this transition, and the separate peaks in the loss data indicate that both peaks are ferroic in origin. Existing thermodynamic predictions for films in equal in-plane tensile strain predict two phase transitions that would affect both principal in-plane orientations in the same way: a ferroelectric transition at higher temperatures with an antiferrodistortive phase transition (AFD) corresponding to the 105 K transition in bulk unstrained $SrTiO_3$ at lower temperatures.[27,28] The antiferrodistortive transition entails a rotation of the TiO_6 octahedra and typically does not have a strong signature in the dielectric properties.[29]

To further probe the nature of T_1 and T_2, the switchable polarization was measured as a function of temperature for the two principal axes (see Fig. 2). It is clear that the onset of reversible polarization occurs at two different temperatures along the two principal in-plane directions. The shorter in-plane axis develops a switchable polarization ~40 K below the onset of polarization along the longer (more strained) axis. Thus, both T_1 and T_2 are ferroelectric in origin. The fact that a switchable polarization develops at different temperatures along the principal in-plane directions and that there are two observed T_{max} as a function of angle suggests that T_1 corresponds to the development of a ferroelectric phase with the polarization parallel (or nearly so) to the long axis in this fully coherent film. T_2 would then correspond to a ferroelectric-ferroelectric phase transition in which either the polarization rotates away from the longer axis or one in which an independent polarization component develops along the shorter axis.

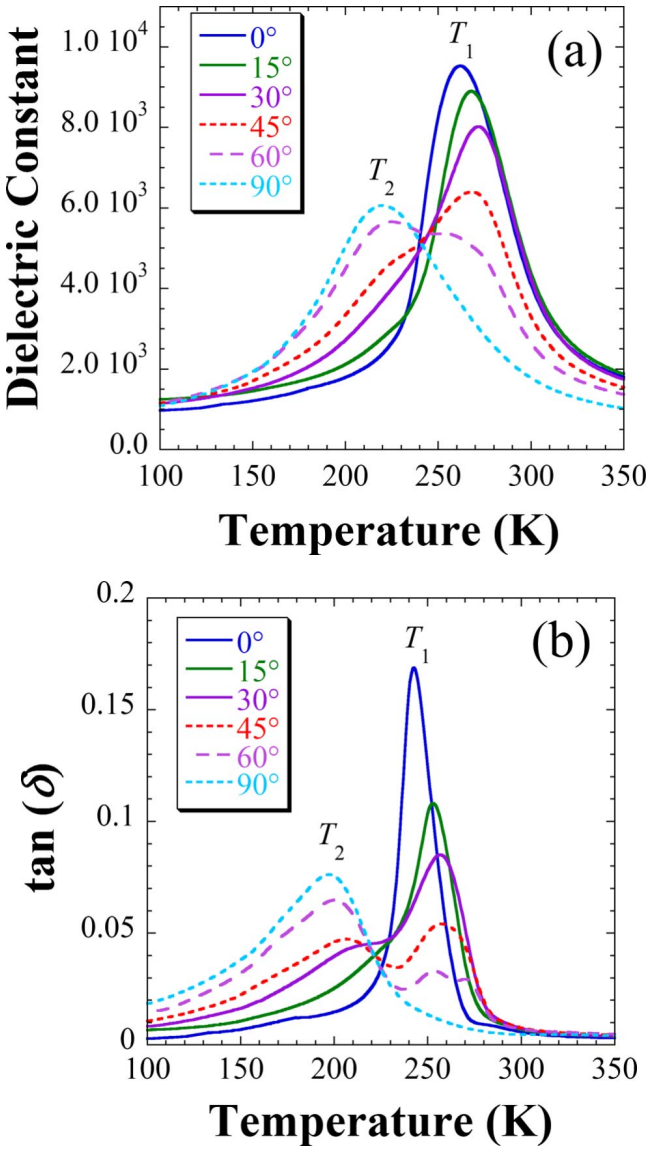

FIG. 1. (Color online) In-plane dielectric permittivity at 5 kHz of a 250 Å thick $SrTiO_3$ thin film measured as a function of temperature for several in-plane angles showing two distinct peaks (T_1 and T_2) sampled as a function of angle. 0° is aligned with the longer $[010]_p$ $SrTiO_3$ axis (parallel to [010] $DyScO_3$), and 90° is aligned along the shorter $[100]_p$ $SrTiO_3$ (parallel to $[10\bar{1}]$ $DyScO_3$).

Previously, Chang *et al.*[30] reported a difference in T_{max} between the two principal in-plane axes for $SrTiO_3$ thin films on $DyScO_3$, though only a ~5 K difference was observed in that work. The discrepancy can be attributed to two factors. First, the initial batch of (101) $DyScO_3$ substrates on which

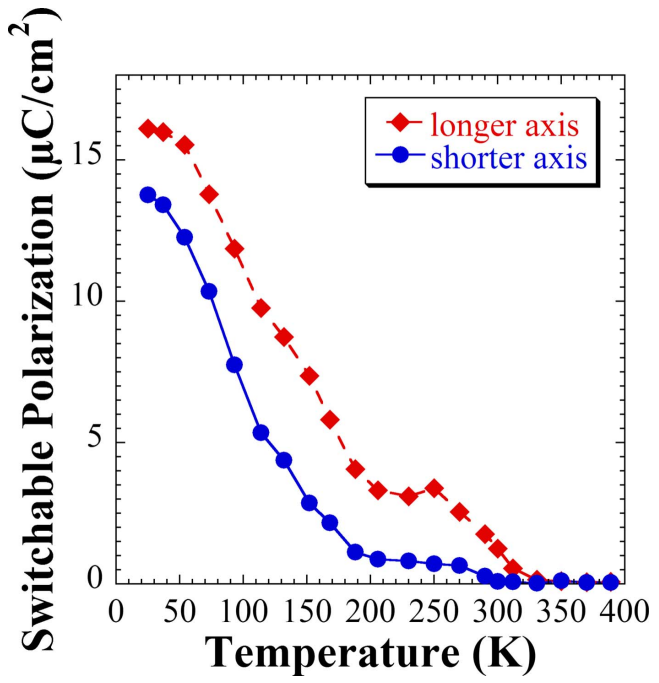

FIG. 2. (Color online) Switchable polarization as a function of temperature for the two principal in-plane directions of the 250 Å thick $SrTiO_3$ film on (101) $DyScO_3$.

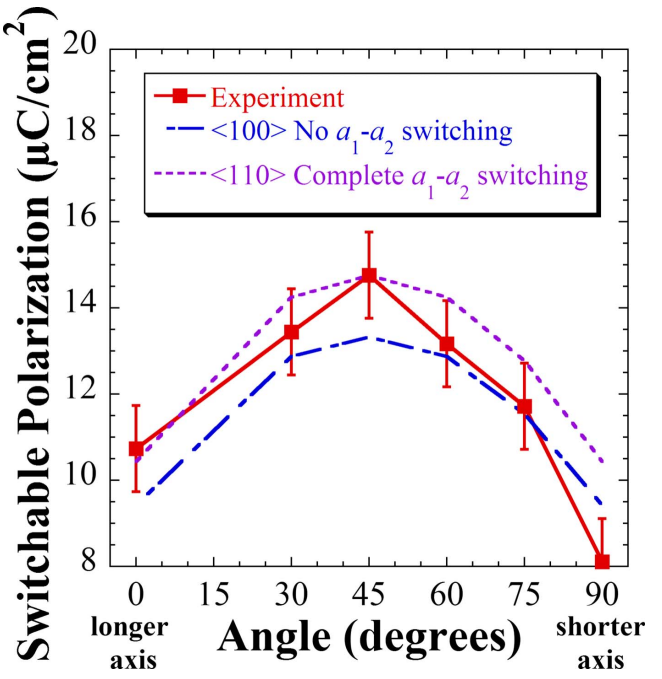

FIG. 3. (Color online) Switchable polarization measured as a function of in-plane angle from the longer (more strained) axis at 70 K for a 250 Å thick $SrTiO_3$ film. The experimental data (■) is shown with the solid line and the models are shown with dashed lines.

their film was grown was later observed to have a small percentage of twins (<1%). This would complicate any determination of the orientation dependence. Second, the structural quality of the initial (101) $DyScO_3$ substrates is poorer than that of the substrates used in this study. The films on the early crystals have rocking curve widths of 0.004° (as described in Ref. 11), whereas the rocking curve widths here were 0.0019° and 0.0018° for the 500 and 250 Å thick films, respectively. Given the pre-existing defects, it is not surprising that the stain state of the films in Ref. 36 would be closer to thermodynamic equilibrium. For films thicker than the critical thickness (~100 Å by Matthews Blakeslee criterion[14,31]) films on defective substrates should be more relaxed.[32] In general, it is observed that the strain along the longer axis relaxes more rapidly than the strain in the shorter in-plane direction.[14] This is consistent with prior reports of homogeneous strain stated for thicker $SrTiO_3$ films grown on (101) $DyScO_3$.[11,12,35,36] The asymmetry between the two $\langle 100\rangle_p$ in-plane lattice parameters was determined to be 0.0005 ± 0.0004 Å for the 500 Å thick film in Refs. 11, 12, 34, and 36. The 500 Å thick film examined in this work, however, has an asymmetry of 0.0014 ± 0.0004 Å. The asymmetry of the dielectric tunability reported by Chang *et al.*[36] is consistent with a lower dielectric maximum along the shorter in-plane direction since tunability is generally higher near the peak permittivity. $Ba_{0.60}Sr_{0.40}TiO_3$ (Ref. 33) and $Pb_{0.35}Sr_{0.65}TiO_3$ films on (101) $NdGaO_3$ (isostructural to $DyScO_3$) have also been shown to possess asymmetry in their in-plane dielectric properties.[34]

2. Orientation dependence of ferroelectric polarization

To examine the anisotropy in the polarization in more depth, the dependence of the switchable polarization as a function of orientation was studied at 70 K, where both principal axes are ferroelectric (see Fig. 3). A peak in the switchable polarization appears approximately 45° away from either principal axis. This is clearly inconsistent with $\langle 100\rangle_p$ as the polar axis if complete a_1-a_2 in-plane switching is allowed. Such a scenario should have maximum in the switchable polarization at 0° and 90° with a minimum near 45°. Thus, other possibilities were considered. Figure 3 compares the experimentally measured dependence of the switchable polarization to two models. One model assumes that the polar direction is parallel to $\langle 100\rangle_p$, but with two different polarizations along $[100]_p$ and $[010]_p$. In this case, to get the polarization maximum near 45° it was assumed that the volume fractions of a_1 and a_2 domains were equal and that little a_1-a_2 switching is possible. The polarization components along the two principal in-plane directions are taken from the experimental data. The second model assumes that the polarization at low temperatures is along $\langle 110\rangle_p$ and that a_1-a_2 switching is possible. Again the polarization along $[110]_p$ is taken from the experimental data. As can be seen in Fig. 3, both models describe the angular dependence of the switchable polarization equally well.

Previously, SHG measurements on partially relaxed $SrTiO_3$ films on $DyScO_3$, where the strain state is approximately uniform in plane ($\varepsilon_{100}=0.93 \pm 0.02\%$ and $\varepsilon_{010}=0.95 \pm 0.02\%$), were used to conclude that the polarization is parallel to $\langle 110\rangle_p$ from 77 K to room temperature.[35] In coherent and anisotropically strained $SrTiO_3$/(101) $GdScO_3$ films, SHG measurements suggest multiple polarization rotation transitions with temperature as the remanent polarization rotates between $[100]_p$ and $[\ell 10]_p$ $(0<\ell<1)$.[36] Compa-

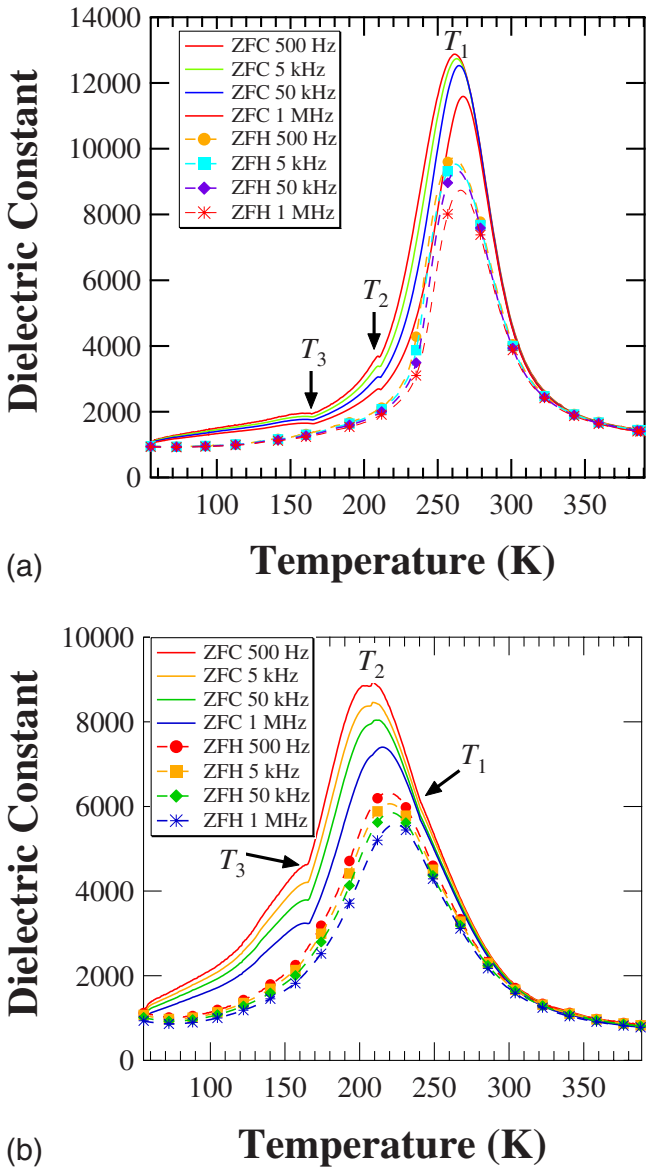

FIG. 4. (Color online) In-plane dielectric constant of a 250 Å thick film measured on zero-field heating and cooling for (a) along the longer in-plane direction and (b) along the shorter in-plane direction showing signatures of three peaks in both principal directions.

rable measurements on $SrTiO_3/(101)$ $DyScO_3$ coherent films are presented here, where the strains state is anisotropic in-plane.

3. Evidence for three transitions

The temperature dependence of the real part of the dielectric constant of $\varepsilon'(T)$ shows considerable thermal hysteresis (Fig. 4). On zero-field cooling (ZFC) below T_{max}, the $SrTiO_3$ shows much more frequency dispersion in the permittivity and a larger dielectric constant than when measured on zero-field heating (ZFH). This suggests that these $SrTiO_3$ films spontaneously develop (at least partially) a ferroelectric macrodomain state at low temperatures. The result of the appearance of a more normal ferroelectric state is reduced dielectric dispersion, a reduced magnitude of the permittivity, and a shift of the peak in the permittivity to slightly higher temperatures, all of which are apparent in Fig. 4. The spontaneous development of a normal ferroelectric state without the application of a dc bias field does not occur in all relaxors, but has been previously reported for lead scandium tantalate ceramics with low point-defect concentrations.[37] It is also reasonable that the permittivity data for ZFC and ZFH converge above T_{max} where the ferroelectric phase is destabilized.[38,39]

From Fig. 4 it can also be seen that there are three dielectric anomalies for measurements along both in-plane $\langle 100 \rangle_p$ directions. This indicates that all of the transitions occur regardless of the direction of the small signal electric field implemented in the measurement. This is contrary to the theory suggested by Chang *et al.*,[36] that the differences in T_{max} for the two orthogonal in-plane axes are due to the coupling of the electric field used in the measurement to a x_6 shear tensor. Their theory predicts only a 5 K difference in transition temperature and could not explain the ~40 K splitting observed in our data.

The permittivity anomaly at 165 K (labeled T_3) is present in measurements along both in-plane orthogonal directions. Unlike the transitions at T_1 and T_2, the transition at T_3 shows a relatively small signature in the permittivity. This feature may correspond to the antiferrodistortive transition, predicted by thermodynamics to be between 120 and 175 K for an average strain state like that shown by these films.[8,11]

4. Relaxor nature of transitions

As has previously been reported, these $SrTiO_3$ films on $DyScO_3$ show dispersion in the permittivity sweeps as a function of temperature that is consistent with relaxor ferroelectricity.[40] It is clear from Fig. 4 that dielectric dispersion was observed along both in-plane principal axes, *even for samples below the critical thickness for relaxation.* Thus, the dielectric relaxation is not a function of structural relaxation.

The dielectric relaxor behavior also exhibits an asymmetry associated with the differences in in-plane strain. To contrast the two principal in-plane directions, the power relation described by Martirena and Burfoot was used to fit the permittivity data above T_{max},[41]

$$\frac{1}{\varepsilon(T)} = \frac{1}{\varepsilon_{max}}\left[1 + \frac{[T - T_{max}]^{\gamma}}{2\delta^2}\right], \quad (1)$$

where ε_{max} is the maximum real permittivity, T_{max} is the temperature corresponding to ε_{max}, and γ and δ are fitting constants. γ is a measure of the degree of relaxor ferroelectric character; for $\gamma=1$, Eq. (1) simplifies to the Curie-Weiss law for normal ferroelectrics, and for $\gamma=2$, Eq. (1) becomes the quadratic relation given by Smolensky[42] for ferroelectric relaxors. Thus the closer γ is to 2, the more "relaxor character" the material has. For the ZFC dielectric data measured along the larger in-plane direction, $\gamma=2.00\pm0.03$, while $\gamma=1.78\pm0.03$ for the shorter in-plane axis. Somewhat smaller differences in γ values were observed in other films. In all cases, however, more relaxor character was observed along the long axis.

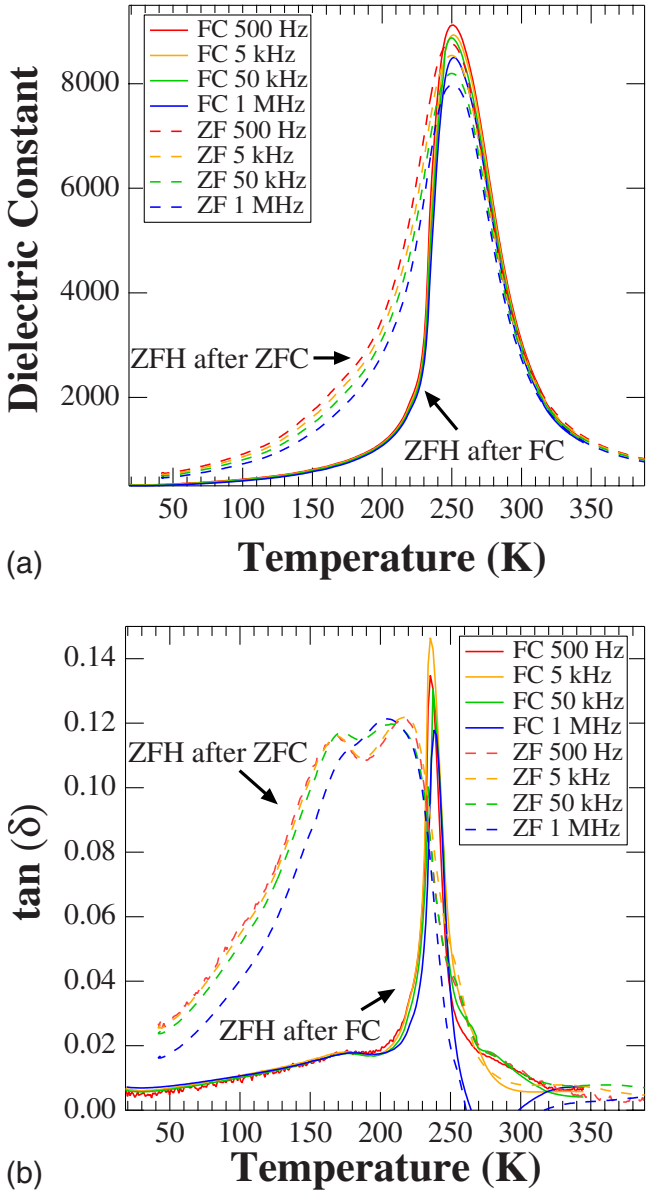

FIG. 5. (Color online) (a) In-plane dielectric constant and (b) loss tangent for the 500 Å thick film measured along the shorter in-plane axis on heating after cooling the films without dc bias (ZF: zero field) represented by dashed lines and under 3 kV/cm dc bias (FC: field cooled) represented by solid lines. All the frequencies collapse after field cooling, indicating a more normal ferroelectric state.

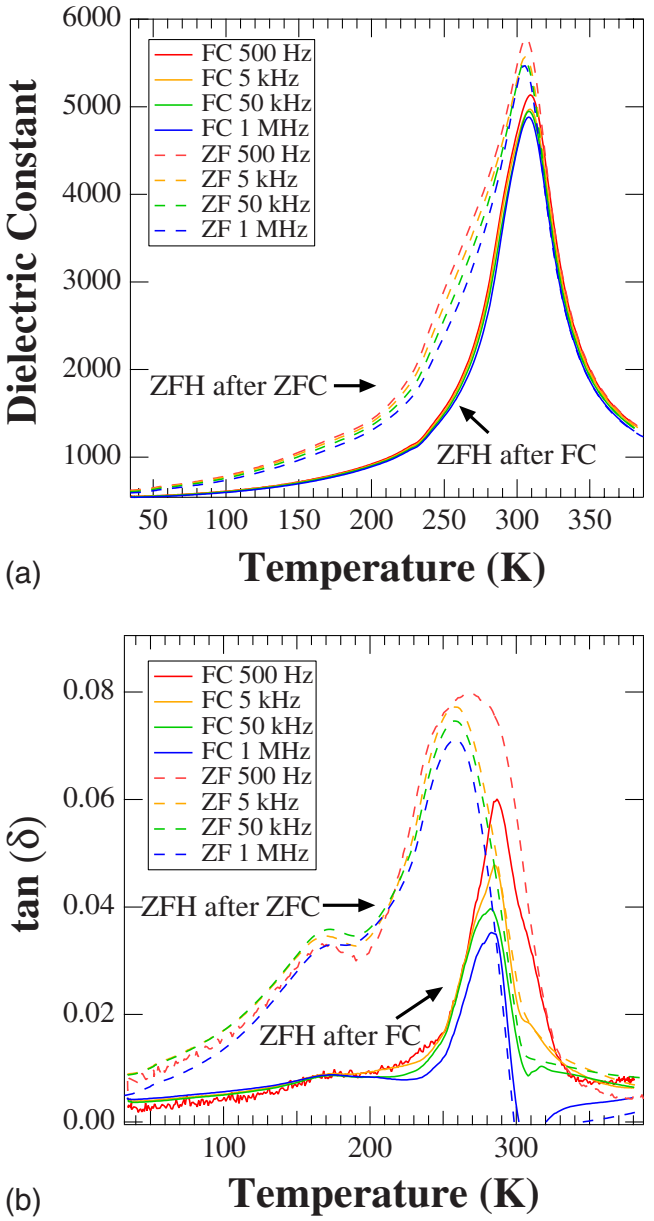

FIG. 6. (Color online) (a) In-plane dielectric constant and (b) loss tangent data measured along the longer axis on heating for a 500 Å thick film cooled without dc bias (ZF: zero field) shown as dashes and under 3 kV/cm dc bias (FC: field cooled) represented by solid lines. There is much less frequency dispersion in the measurement after field cooling, indicating a more normal ferroelectric transition.

This anisotropy of the relaxor character is also present in the field cooling data (Fig. 5). The samples were cooled under an applied dc bias of 3 kV/cm (FC) and the permittivity was measured on heating (ZFH after FC). Upon heating, the dielectric constant shows less frequency dispersion and a slightly higher transition temperature as shown in Figs. 5(a) and 6(a). This indicates that a macrodomain state is induced, which is typical for relaxor materials. Measurements of the field-cooled sample along the shorter axis show the sharpest peak observed in the loss data [Fig. 5(b)]. This is coupled with a collapse of the frequency dependence of the loss. The ability to stabilize a more normal ferroelectric state along the shorter in-plane is consistent with the measured γ's showing a stronger relaxor character along the longer in-plane direction.

5. SHG results on in-plane polarization directions

To help resolve the ambiguity in the direction of the spontaneous polarization in these anisotropically strained films, polarization-dependent SHG measurements were conducted. SHG is a nonlinear process which involves the conversion of a fundamental light of frequency ω to light of frequency 2ω,

as determined by the nonlinear polarization $P_i^{2\omega} \propto d_{ijk} E_j^{\omega} E_k^{\omega}$, where d_{ijk} is a third-rank nonlinear tensor with form similar to that of the piezoelectric tensor.[43] The subscripts i, j, and k refer to the crystal physics axes of the studied thin film. For this case we consider $mm2$ as the symmetry point group based on the fact that both x-ray diffraction and phase-field simulations indicate three different lattice parameters, two within the substrate plane and a third normal to the film surface. According to Neumann's principle, the only contributing (nonzero) nonlinear coefficients of d_{ijk} are d_{15}, d_{24}, d_{31}, d_{32}, and d_{33}. Assuming the twofold rotation axis in the plane of the film, two general models for the direction of ferroelectric polarization are considered.

Model I: the film has polarization along one direction only: either along $x[100]_p$, or along $y[010]_p$, or at an arbitrary angle φ in the plane of the sample.

Model II: the film is composed of domains with twinning, i.e., polarization along two in-plane directions orthogonal to each other. Two cases are considered within model II:

Case I: the sample consists of domains with polarization along $x[100]_p$ (short axis), *and* along $y[010]_p$ (long axis).

Case II: the film is composed of domains with polarization along $x'[110]_p$ *and* along $y'[\bar{1}10]_p$. The validity of each of these models is examined next.

Model I. The domain polarization is assumed to be only along one axis. For polarization along the long axis $y[010]_p$ the following expressions are derived:

$$I_x^{2\omega} = d_{15}^2 \sin^2[2(\theta - \varphi)], \tag{2}$$

$$I_y^{2\omega} = [d_{31} \cos^2(\theta - \varphi) + d_{33} \sin^2(\theta - \varphi)]^2, \tag{3}$$

where φ is a small offset angle that can arise from polarization rotation in the film plane and can also be sensitive to antiferrodistortive rotations.[44] Similar expressions can be derived for polarization along $x[100]_p$. Figures 7(a) and 7(b) show polar plots at $T=175$ K with the analyzer parallel to x and y directions, respectively. Clearly, model I does not fit the experimental data well. Similarly poor fits were obtained at all temperatures studied from ~5–300 K, and hence this model is thus ruled out. Therefore, twinning appears to be present at all temperatures, but as we will see next, the polarization along the long $y[010]_p$ axis does dominate just below T_1.

Model II. Assuming twinned domains with ferroelectric polarizations orthogonal to each other within the film plane, the SHG polar plot intensity can be modeled using the following expression:[45]

$$I_j^{2\omega} = K_{1,j} \sin^2 2(\theta - \varphi) + K_{2,j}[\sin^2(\theta - \varphi) + K_{3,j} \cos^2(\theta - \varphi)]^2 + K_{4,j}[\sin^2(\theta - \varphi) + K_{3,j} \cos^2(\theta - \varphi))\sin 2(\theta - \varphi)], \tag{4}$$

where $j=x,y$ for case I of model II and $j=x',y'$ for case II of model II. $K_{i,j}$ are constants and φ is an offset angle. For case I, the ratios of the net ferroelectric polarization along x and y, $|P_y^{\text{net}}/P_x^{\text{net}}|$, as well as the material property, $|d'_{15}/d_{33}|$ which represents the ratio of nonlinear SHG coefficients, are given by

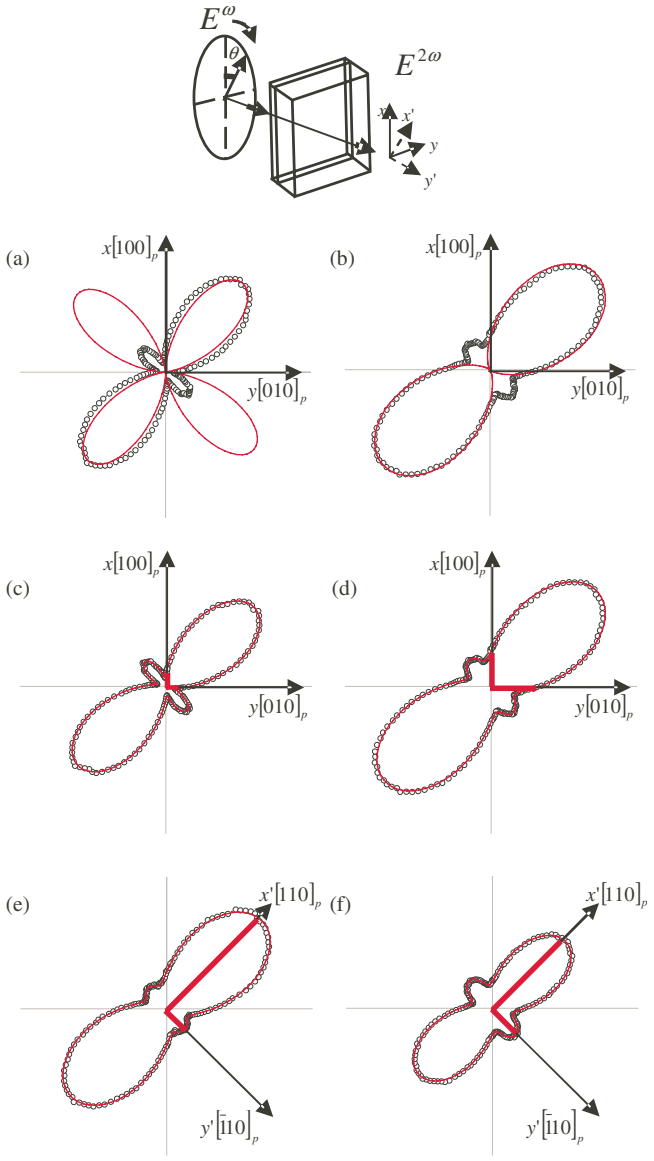

FIG. 7. (Color online) The schematic on the top depicts the second-harmonic generation (SHG) setup where light of frequency ω and linear polarization, at an angle θ with respect to the x axis, is converted to light of frequency 2ω, after interacting with the sample. By varying the angle θ, and fixing an analyzer along the x, y, x', and y' directions SHG intensity polar plots, i.e., $I_x^{2\omega}$, $I_y^{2\omega}$, $I_{x'}^{2\omega}$, and $I_{y'}^{2\omega}$ are obtained. Figures 7(a)–7(f) show SHG polar plots at 175 K. These compare the theoretical models, represented by the thin solid red lines to the experimental data, represented by open circles. In particular, the comparison is the following: (a) *model I* fit, $I_x^{2\omega}$, (b) *model I* fit, $I_y^{2\omega}$ (c) *model II, case I* fit, $I_x^{2\omega}$, (d) *model II, case I* fit, $I_y^{2\omega}$, (e) *model II, case II* fit, $I_{x'}^{2\omega}$, and (f) *model II, case II* fit, $I_{y'}^{2\omega}$. The thick solid red lines in Figs. 7(c)–7(f) represent intensities which must be reciprocal in order for the fitting models to be valid. Clearly, this is true only for Figs. 7(c) and 7(d), based on model II, case I.

$$\left|\frac{P_y^{\text{net}}}{P_x^{\text{net}}}\right|^4 = \left(\frac{K_{1,x}K_{2,y}}{K_{2,x}K_{1,y}}\right)K_{3,y}^2 \tag{5}$$

and

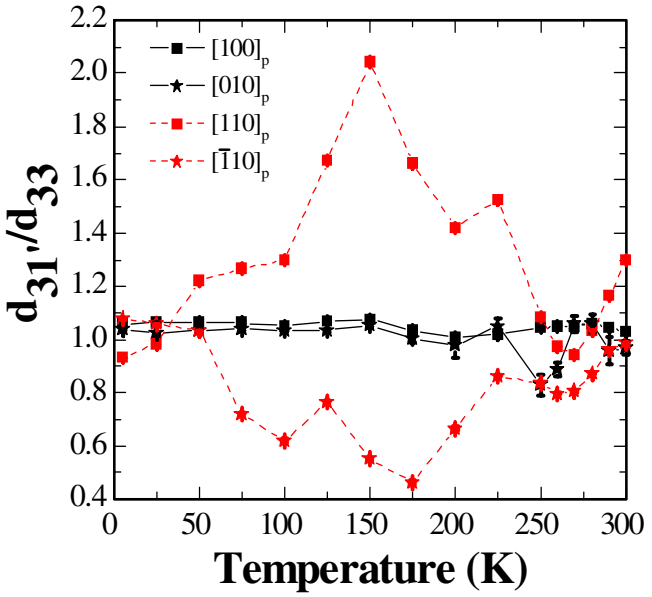

FIG. 8. (Color online) Temperature dependence of the nonlinear coefficient $|d'_{31}/d_{33}|$. Shown here are the quantities that correspond to left- and right-hand sides of Eq. (8) (black solid lines) and Eq. (9) (red dashed lines). For all measured temperatures, Eq. (8) is valid since the left- and the right-hand side quantities are equal (black squares and stars), whereas clearly Eq. (9) is not valid. Since, Eq. (8) is satisfied, we can conclude that the in-plane polarization is along the $\langle 100\rangle_p$ and not the $\langle 110\rangle_p$ directions.

$$\left(\frac{d'_{15}}{d_{33}}\right)^4 = \left(\frac{1}{K_{3,y}}\right)^2 \left(\frac{K_{1,x}K_{1,y}}{K_{2,x}K_{2,y}}\right), \tag{6}$$

where $d'_{15}=(d_{15}+d_{24})/2$. For case II of model II, Eqs. (5) and (6) hold with the substitution of subscripts (x,y) with (x',y').

Case I. Each domain has polarization either along $x[100]_p$ or $y[010]_p$, and both types of domains coexist in a twinned state. From Eq. (4) it can be shown that the following condition should be satisfied:

$$\frac{d'_{31}}{d_{33}} = K_{3,x} = K^{-1}_{3,y}, \tag{7}$$

where $d'_{31}=(d_{31}+d_{32})/2$. Since $K_{3,j}=I_j^{2\omega}(0°)/I_j^{2\omega}(90°)$, the following equality must be satisfied:

$$I_x^{2\omega}(0°)/I_x^{2\omega}(90°) = I_y^{2\omega}(90°)/I_y^{2\omega}(0°). \tag{8}$$

Figures 7(c) and 7(d) show polar plots at $T=175$ K with the analyzer parallel to the x and y directions, respectively. The experimental data (circles) fit very well with the theoretical model (solid lines). In addition, $I_x^{2\omega}(0°)/I_x^{2\omega}(90°)\sim(1.02)^2$ and $I_y^{2\omega}(90°)/I_y^{2\omega}(0°)\sim 1^2$ are in excellent agreement. Figure 8 is a graphical representation of Eq. (8) and it shows that the equality is consistently valid for the entire measured temperature range as seen from the two black curves (black squares and stars) representing, respectively, the right and left sides of Eq. (8).

Case II. The domain polarization is along $x'[110]_p$ or $y'[\bar{1}10]_p$ and both domains coexist in a twinned state. The following required condition is obtained:

$$I_{x'}^{2\omega}(45°)/I_{x'}^{2\omega}(135°) = I_{y'}^{2\omega}(135°)/I_{y'}^{2\omega}(45°) \tag{9}$$

Figures 7(e) and 7(f) show polar plots at $T=175$ K with the analyzer parallel to the x' and y' directions, respectively. Even though the shape of the fit is overall good, the equality condition defined in Eq. (9) is *not* satisfied since $I_{x'}^{2\omega}(45°)/I_{x'}^{2\omega}(135°)\sim(1.23)^2$ and $I_{y'}^{2\omega}(135°)/I_{y'}^{2\omega}(45°)\sim(0.74)^2$. Upper and lower dashed lines in Fig. 8 shows the left and right sides of Eq. (9) (respectively as squares and stars), as a function of temperature; clearly the equality is *not* satisfied. Based on this analysis we can conclude that the direction of the ferroelectric polarization of the film is along $\langle 100\rangle_p$. The films are twinned into the two in-plane domain states.

The temperature dependence of $I_y^{2\omega}(0^0)$ is shown in Fig. 9(a). Its behavior is very similar to that of the spontaneous polarization along the long axis as shown in Fig. 2 for macroscopic electrical measurements. On the other hand, Fig. 9(b) shows the temperature dependence of $|P_y^{\text{net}}/P_x^{\text{net}}|$. At room temperature the ratio is $\sim 5:1$ and it reaches a peak of $\sim 7:1$ at approximately 260 K, where the domain fraction with the net polarization along the long axis dominates the domain fraction with the net polarization along the short axis. This is in agreement with the electrical measurements in Fig. 2. As the temperature is further reduced, the ratio starts to drop and reaches a constant value of ~ 1 for $T<175$ K. This implies that for $T<175$ K, the probed area has approximately equal fraction of domains with polarization along $x[100]_p$ and $y[010]_p$.

The ratio of the nonlinear coefficients, $|d'_{15}/d_{33}|$, which is an intrinsic property of the film, is plotted as a function of temperature in Fig. 9(c). There is a clear anomaly at 175 K, which can be associated with the antiferrodistortive transition of the thin film. Furthermore, Fig. 9(d) shows the offset angle φ as a function of temperature. For $T>200$ K the offset is non existent. However, at $T<175$ K a small rotation of $\sim 1.6°$ appears. This offset persists until the lowest temperature and can therefore likely be attributed to the AFD transition of the film, as shown in the dielectric response, and which was predicted to occur between 120 and 175 K.[8,11] This offset arises from the coupling of the antiferrodistortion to the SHG signal.[44]

IV. THERMODYNAMIC ANALYSIS AND PHASE-FIELD SIMULATIONS

To understand the in-plane directional dependence of the dielectric, ferroelectric, and SHG measurements for $SrTiO_3$ on $DyScO_3$, we conducted both thermodynamic analysis and phase-field simulations, similar to Refs. 11 and 12, taking into account the asymmetric substrate strain. The expressions for the bulk free-energy density f_{bulk} and the elastic energy density f_{elastic} are the same as in Ref. 12. It is important to note that the thermodynamic description utilized here does not treat the relaxor ferroelectric character, but is expected to provide a reasonable description of the ferroic phase transi-

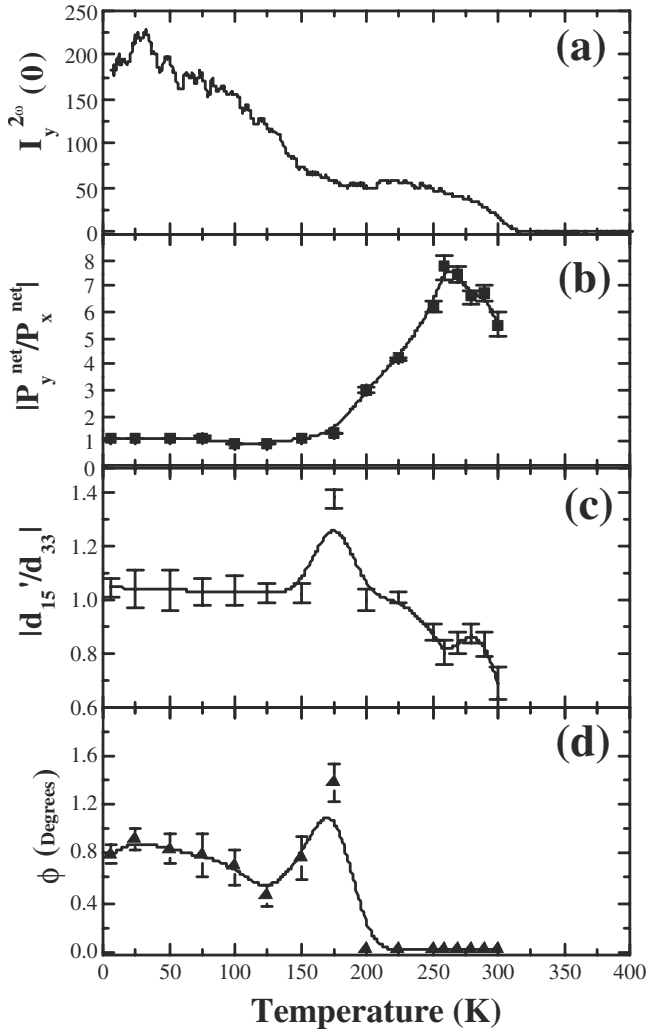

FIG. 9. Shown here is the temperature dependence of (a) second-harmonic intensity with a fixed analyzer along the y direction and $\theta=0°$, i.e., $I_y^{2\omega}(0°)$ and (b) the absolute ratio of the net polarization along the y axis to the net polarization along the x axis, $|P_y^{net}/P_x^{net}|$ Both (a) and (b) are in good agreement with the electrical measurements of the polarization in Fig. 2. Figure 9(c) shows the temperature dependence of the nonlinear coefficient ratio $|d_{15}'/d_{33}|$ and Fig. 9(d) shows the offset angle (φ) from the polar plot fitting as a function of temperature. Both show an anomaly at 175 K that can be most likely attributed to the AFD transition.

tions. The thermodynamic calculations and phase-field simulations were performed by simply replacing $\bar{\varepsilon}_{11}=\bar{\varepsilon}_{22}=e_0$ by $\bar{\varepsilon}_{11}=e_{s1}$ and $\bar{\varepsilon}_{22}=e_{s2}$ ($e_{s1}\neq e_{s2}$, the biaxial strains) in the previous work (Ref. 12) while the description of the modeling and parameters used remain valid.

As shown in Ref. 12 for the case of symmetric strains, the variations in the reported values of bulk properties and in the Landau energy coefficients from different literature sources lead not only to a wide range of possible transition temperatures at a given strain, but also to different ferroelectric states (e.g., polarization along the pseudocubic $[110]_p$ vs $[100]_p$ directions), and thus different domain structures under a biaxial tensile strain.[12] For the case of an asymmetric strain with $e_{s1}=1.03\%$ along the [100] axis and $e_{s2}=1.06\%$ along the [010] axis, the transition temperatures determined from thermodynamic calculations and phase-field simulations are summarized in Table I for two different values of α_{12} in the Landau free-energy expression from the literature,[8,46,47] together with the experimental measurements. For both cases, there are three transition temperatures as a result of the asymmetric strain. The representative domain structures after each of the three transitions for both $\alpha_{12}=5.5\times10^{-12}$ cm^6 dyn/esu^4 and $\alpha_{12}=1.7\times10^{-12}$ cm^6 dyn/esu^4 are shown in Fig. 10. In Table I and Fig. 10, we use p_i and q_i to represent polarization components and antiferrodistortive structural order parameters, respectively. On cooling from room temperature, the first ferroelectric transition (T_1) corresponds to the development of a polarization along the longer in-plane direction (i.e., the higher strain axis, here $[010]_p$ axis), while the lowest transition (T_3) is due to the antiferrodistortive structural transition in the $SrTiO_3$. However, for the intermediate transition temperature (T_2), the two coefficients (α_{12}) in the Landau free energy led to two different ferroelectric states, $[010]_p/[100]_p$ polar states for $\alpha_{12}=5.5\times10^{-12}$ cm^6 dyn/esu^4 and $[110]_p/[1\bar{1}0]_p$ for $\alpha_{12}=1.7\times10^{-12}$ cm^6 dyn/esu^4 (see Table I and Fig. 10). For the case of $\alpha_{12}=5.5\times10^{-12}$ cm^6 dyn/esu^4, the additional transition (T_2) is due to twinning from a single variant $[010]_p$ to $[010]_p/[100]_p$ domain structure. Since the overall average strain is tensile, a twin structure is favorable over a single variant ferroelectric state. Therefore, for $\alpha_{12}=5.5\times10^{-12}$ cm^6 dyn/esu^4, it is the competing elastic interactions between the in-plane domain variants that favor the twin formation and the asymmetric substrate constraint which prefers a single domain state that leads to an addi-

TABLE I. Predicted transition temperatures from thermodynamics and phase-field simulations

	$\alpha_{12}=5.5\times10^{-12}$ cm^6 dyn/esu^4		$\alpha_{12}=1.7\times10^{-12}$ cm^6 dyn/esu^4		
	Thermodynamics	Phase field	Thermodynamics	Phase field	Experiments
T_1	224 K	212 K	224 K	214 K	~260 K
	$(0,p_2,0)$	$(0,p_2,0)$	$(0,p_2,0)$	$(0,p_2,0)$	
T_2	Not available[a]	200 K	216 K	210 K	~210 K
		$(p_1,0,0)+(0,p_2,0)$	$(p_1,p_2,0)$	$(p_1,p_2,0)$	
T_3	112 K	113 K	113 K	114 K	~160 K
	$(0,p_2,0,)+(q_1,0,0)$	$(p_1,0,0)+(0,p_2,0)+(q_2,0,0)+(0,q_1,0)$	$(p_1,p_2,0)+(q_1,q_2,0)$	$(p_1,p_2,0)+(q_1,q_2,0)$	

[a]For $\alpha_{12}=5.5\times10^{-12}$ cm^6 dyn/esu^4 the $(0,p_2,0)$ phase is always stable by thermodynamic analysis under the single domain assumption.

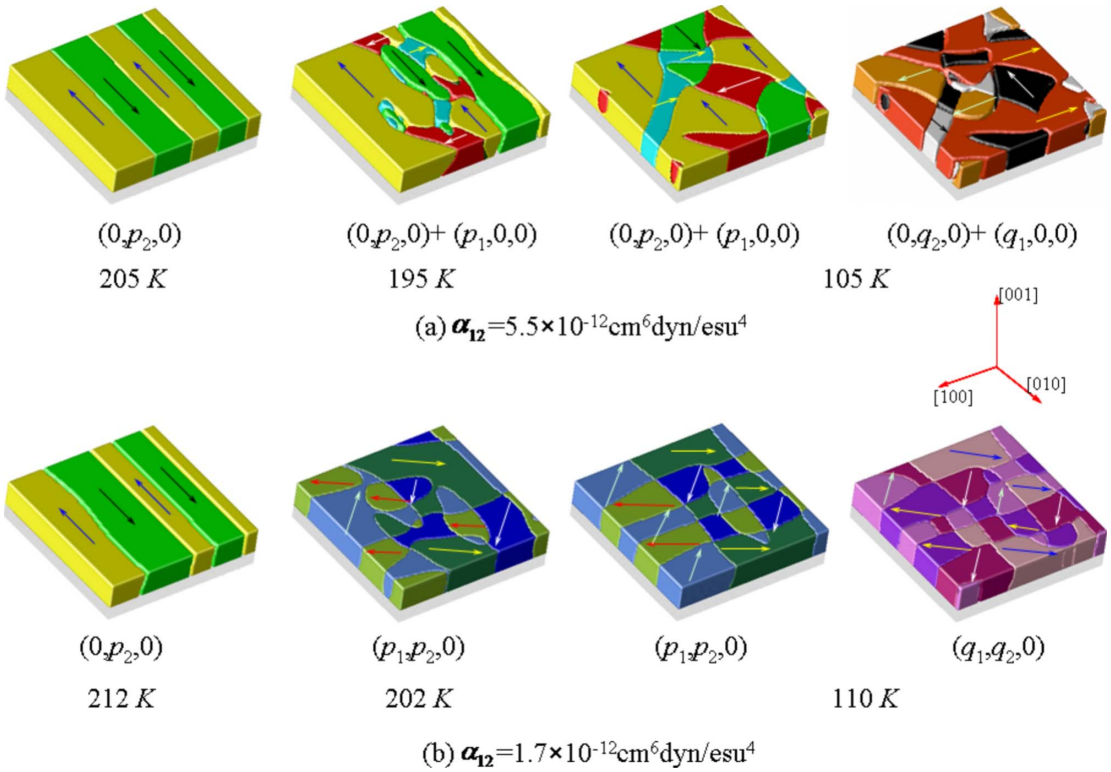

FIG. 10. (Color online) Representative domain structures from phase-field simulations following each of the three transitions for (a) $\alpha_{12}=5.5\times10^{-12}$ cm^6 dyn/esu^4 and (b) $\alpha_{12}=1.7\times10^{-12}$ cm^6 dyn/esu^4. Different colors are used to identify the four kinds of domain variants for both (100) and (110) polar states and the directions of the vectors p and q are shown by the arrows.

tional phase transition as compared to the symmetric strain case. For $\alpha_{12}=1.7\times10^{-12}$ cm^6 dyn/esu^4, the second phase transition produces a polar state along the $[110]_p$ direction, the stable polar state under an equivalent symmetric strain. The fact that our prior SHG and confocal scanning optical microscopy measurements of $SrTiO_3$ films at slightly different but symmetric strains exhibit polar directions along the pseudocubic $[110]_p$ directions while the present SHG measurements of asymmetrically strained films showed that the $[100]_p$ polar states indicates a small difference in thermodynamic stability of the $[110]_p$ and $[100]_p$ polar states. Therefore, an accurate prediction of polar states for different strain states will require more precise values of Landau coefficients than the existing ones. Despite the different polar states for the second phase transition (T_2) due to the uncertainty in the Landau coefficients, it does not change the conclusion that the anisotropic strain causes the additional phase transition as compared to the symmetric strain case. It should also be pointed out the temperature range for the single variant state predicted from thermodynamics and phase-field simulations for either α_{12} is significantly smaller than that measured in the experiment.

There are several factors that could lead to the observed discrepancies in the absolute temperatures of the transition between theory and experiment. First, the differences may result from the uncertainty in the values of the materials constants input into the model. Typically the uncertainty in these values result in error bars on the calculated transition temperature that are similar to the discrepancies observed in this case.[10–12] Furthermore, the values of all these physical constants are assumed to be identical to those for bulk materials, which may or may not be a valid assumption.[11,12,40] Third, the model assumes that the $SrTiO_3$ film is a normal ferroelectric, but it has been clearly shown that the strained $SrTiO_3$ behaves like a relaxor ferroelectric. Introduction of relaxor character to the material often shifts the temperature of the maximum permittivity by tens of degrees. A classical example here is found in $Pb(Sc,Nb)O_3$ and $Pb(Sc,Ta)O_3$, where the relaxor nature can be controlled by the disorder in the system and changed by a high-temperature anneal. In these systems, annealing can shift the peak of the dielectric constant 30 K.[48–50]

V. CONCLUSIONS

Asymmetrically strained $SrTiO_3$ shows two distinct permittivity maxima along the $SrTiO_3$ $[100]_p$ and $[010]_p$ directions. Measurements of the switchable polarization as a function of temperature, relaxor character, permittivity after field cooling, and optical second-harmonic generation measurements confirm that that these two features are distinct and real. The higher temperature transition is due to the development of a ferroelectric polarization predominantly along the longer in-plane axis $y[010]_p$, whereas the lower is associated with a ferroelectric-ferroelectric transition in which the polarization orientation develops along both the $y[010]_p$ and the $x[100]_p$ directions. The antiferrodistortive transition near 170 K is observed along both axes with both dielectric and SHG techniques. The thermodynamic modeling confirms that the experimentally observed anisotropy in the properties

can be attributed to the anisotropic strain state of the film. Considering that the anisotropically strained thin films show significantly different domain structure and phase-transition behavior from isotropically strained thin films, we believe that engineering strain anisotropy in ferroelectrics can be an important parameter in controlling the dielectric and ferroelectric properties of thin films.

ACKNOWLEDGMENTS

This work was supported by the National Science Foundation (NSF) under Grant Nos. DMR-0507146, DMR-0602770, and DMR-0820404 and by the Division of Scientific User Facilities, Office of Basic Energy Sciences, U.S. Department of Energy.

[1] A. F. Devonshire, Philos. Mag. **3**, 85 (1954).
[2] D. Bancroft, Phys. Rev. **53**, 587 (1938).
[3] P. W. Forsbergh, Jr., Phys. Rev. **93**, 686 (1954).
[4] G. A. Samara, Ferroelectrics **2**, 277 (1971).
[5] G. A. Rossetti, K. Kushida, and L. E. Cross, Appl. Phys. Lett. **59**, 2524 (1991).
[6] K. Abe, N. Yanase, K. Sano, M. Izuha, N. Fukushima, and T. Kawakubo, Integr. Ferroelectr. **21**, 197 (1998).
[7] N. A. Pertsev, A. G. Zembilgotov, and A. K. Tagantsev, Phys. Rev. Lett. **80**, 1988 (1998).
[8] N. A. Pertsev, A. K. Tagantsev, and N. Setter, Phys. Rev. B **61**, R825 (2000); **65**, 219901(E) (2002).
[9] S. K. Streiffer, J. A. Eastman, D. D. Fong, C. Thompson, A. Munkholm, M. V. Ramana Murty, O. Auciello, G. R. Bai, and G. B. Stephenson, Phys. Rev. Lett. **89**, 067601 (2002).
[10] K. J. Choi, M. D. Biegalski, Y. L. Li, A. Sharan, J. Schubert, R. Uecker, P. Reiche, Y. B. Chen, X. Q. Pan, V. Gopalan, L.-Q. Chen, D. G. Schlom, and C. B. Eom, Science **306**, 1005 (2004).
[11] J. H. Haeni, P. Irvin, W. Chang, R. Uecker, P. Reiche, Y. L. Li, S. Choudhury, W. Tian, M. E. Hawley, B. Craigo, A. K. Tagantsev, X. Q. Pan, S. K. Streiffer, L. Q. Chen, S. W. Kirchoefer, J. Levy, and D. G. Schlom, Nature (London) **430**, 758 (2004).
[12] Y. L. Li, S. Choudhury, J. H. Haeni, M. D. Biegalski, A. Vasudevarao, A. Sharan, H. Z. Ma, J. Levy, V. Gopalan, S. Trolier-McKinstry, D. G. Schlom, Q. X. Jia, and L. Q. Chen, Phys. Rev. B **73**, 184112 (2006).
[13] D. G. Schlom, L.-Q. Chen, C.-B. Eom, K. M. Rabe, S. K. Streiffer, and J.-M. Triscone, Annu. Rev. Mater. Res. **37**, 589 (2007).
[14] M. D. Biegalski, D. D. Fong, J. A. Eastman, P. H. Fuoss, R. Uecker, P. Reiche, W. Tian, X. Q. Pan, M. E. Hawley, S. K. Streiffer, S. Trolier-McKinstry, and D. G. Schlom, J. Appl. Phys. **104**, 114109 (2008).
[15] M. D. Biegalski, J. H. Haeni, C. D. Brandle, A. J. Ven Gratis, S. Trolier-McKinstry, and D. G. Schlom, J. Mater. Res. **20**, 952 (2005).
[16] R. Uecker, B. Velickov, D. Klimm, R. Bertram, M. Bernhagen, M. Rabe, M. Albrecht, R. Fornar, and D. G. Schlom, J. Cryst. Growth **310**, 2649 (2008).
[17] B. Veličkov, V. Kahlenberg, R. Bertram, and M. Bernhagen, Z. Kristallogr. **222**, 466 (2007).
[18] R. P. Liferovich and R. H. Mitchell, J. Solid State Chem. **177**, 2188 (2004).
[19] D. G. Schlom, L. Q. Chen, X. Q. Pan, A. Schmehl, and M. A. Zurbuchen, J. Am. Ceram. Soc. **91**, 2429 (2008).
[20] J. H. Haeni, C. D. Theis, and D. G. Schlom, J. Electroceram. **4**, 385 (2000).
[21] *Thermophysical Properties of Matter Vol. 13: Thermal Expansion of Nonmetallic Solids*, edited by Y. S. Touloukian, R. K. Kirby, R. E. Taylor, and T. Y. R. Lee (Plenum, New York, 1977), p. 288.
[22] O. G. Vendik, S. P. Zubko, and M. A. Nikolskii, Zh. Tekh. Fiz. **69**, 1 (1999); [Tech. Phys. **44**, 349 (1999)].
[23] T. Schmitz, S. Tiedke, and U. Ellerkmann, Integr. Ferroelectr. **67**, 125 (2004).
[24] Throughout this manuscript we use the standard setting of space group 62, *Pnma*, to describe the crystallography of $DyScO_3$. Although some authors use this setting, many others use the nonstandard setting *Pbnm* for $DyScO_3$, and other perovskites with the $GdFeO_3$ crystal structure. The conversion from axes a, b, and c, directions $[a\ b\ c]$, or planes $(a\ b\ c)$ in *Pnma* to a', b', c', $[a'b'c']$, or $(a'b'c')$ in *Pbnm* is given by $a'=c$, $b'=a$, and $c'=b$.
[25] *International Tables for Crystallography, Vol. A: Space Group Symmetry*, 5th ed., edited by T. Hahn (Kluwer, Dordrecht, 2002), p. 66.
[26] *Numerical Data and Functional Relationships in Science and Technology*, edited by K.-H. Hellwege and A. M. Hellwege, Landolt-Börnstein, New Series, Group III, Vol. 7e (Springer, Berlin, 1976), pp. 11–13.
[27] H. Unoki and T. Sakudo, J. Phys. Soc. Jpn. **23**, 546 (1967).
[28] P. A. Fleury, J. F. Scott, and J. M. Worlock, Phys. Rev. Lett. **21**, 16 (1968).
[29] K. A. Müller and H. Burkard, Phys. Rev. B **19**, 3593 (1979).
[30] W. Chang, S. W. Kirchoeffer, J. A. Bellotti, S. B. Qadri, J. H. Haeni, D. G. Schlom, and J. M. Pond, J. Appl. Phys. **98**, 024107 (2005).
[31] J. W. Matthews and A. E. Blakeslee, J. Cryst. Growth **27**, 118 (1974).
[32] L. B. Freund and S. Suresh, *Thin Films Materials: Stress, Defect Formation and Surface Evolution* (Cambridge University Press, Cambridge, 2003), pp. 464–488.
[33] W. K. Simon, E. K. Akdogan, J. A. Bellotti, and A. Safari, Appl. Phys. Lett. **87**, 082906 (2005).
[34] Y. Lin, X. Chen, S. W. Liu, C. L. Chen, J.-S. Lee, Y. Li, Q. X. Jia, and A. Bhalla, Appl. Phys. Lett. **84**, 577 (2004).
[35] A. Vasudevarao, A. Kumar, L. Tian, J. H. Haeni, Y. L. Li, C.-J. Eklund, Q. X. Jia, R. Uecker, P. Reiche, K. M. Rabe, L. Q. Chen, D. G. Schlom, and V. Gopalan, Phys. Rev. Lett. **97**, 257602 (2006).
[36] A. Vasudevarao, S. Denev, M. D. Biegalski, Y. L. Li, L. Q. Chen, S. Trolier-McKinstry, D. G. Schlom, and V. Gopalan, Appl. Phys. Lett. **92**, 192902 (2008).
[37] F. Chu, I. Reaney, and N. Setter, J. Appl. Phys. **77**, 1671 (1995).
[38] L. E. Cross, Ferroelectrics **76**, 241 (1987).
[39] D. Viehland, J. F. Li, S. J. Jang, L. E. Cross, and M. Wuttig,

Phys. Rev. B **46**, 8013 (1992).
[40] M. D. Biegalski, Y. Jia, V. Sherman, S. K. Streiffer, R. Uecker, P. Reiche, D. G. Schlom, and S. Trolier-McKinstry, Appl. Phys. Lett. **88**, 192907 (2006).
[41] H. T. Martirena and J. C. Burfoot, Ferroelectrics **7**, 151 (1974).
[42] G. A. Smolensky, J. Phys. Soc. Jpn. **28**, 26 (1970).
[43] Y. R. Shen, *The Principles of Nonlinear Optics* (Wiley, New York, 2003), p. 86.
[44] S. Denev, A. Kumar, M. D. Biegalski, H. W. Jang, C. M. Folkman, A. Vasudevarao, Y. Han, I. M. Reaney, S. Trolier-McKinstry, C.-B. Eom, D. G. Schlom, and V. Gopalan, Phys. Rev. Lett. **100**, 257601 (2008).
[45] A. Sharan, J. Lettieri, Y. Jia, W. Tian, X. Pan, D. G. Schlom, and V. Gopalan, Phys. Rev. B **69**, 214109 (2004).
[46] H. Uwe and T. Sakudo, Phys. Rev. B **13**, 271 (1976).
[47] A. K. Tagantsev, E. Courtens, and L. Arzel, Phys. Rev. B **64**, 224107 (2001).
[48] C. G. F. Stenger, F. L. Scholten, and A. J. Burggraaf, Solid State Commun. **32**, 989 (1979).
[49] N. Setter and L. E. Cross, J. Mater. Sci. **15**, 2478 (1980).
[50] F. Chu, I. M. Reaney, and N. Setter, J. Appl. Phys. **77**, 1675 (1995).